A minimal passive model of the operational amplifier: application to Sallen–Key analog filters

Müller Remy, Thomas Hélie

A MINIMAL PASSIVE MODEL OF THE OPERATIONAL AMPLIFIER : APPLICATION TO SALLEN-KEY ANALOG FILTERS

Rémy Müller

IRCAM-STMS (UMR 9912)
Sorbonne University
Paris, France
remy.muller@ircam.fr

Thomas Hélie *

IRCAM-STMS (UMR 9912)
Sorbonne University
Paris, France
thomas.helie@ircam.fr

ABSTRACT

This papers stems from the fact that, whereas there are passive models of transistors and tubes, a minimal passive model of the operational amplifier does not seem to exist. A new behavioural model is presented that is memoryless, fully described by its interaction ports, with a minimal number of equations, for which a passive power balance can be defined. The proposed model handles saturation, asymmetric power supply, and can be used with non-ideal voltage references. To illustrate the model in audio applications, the non-inverting voltage amplifier and a saturating Sallen-Key lowpass filter are considered.

1. INTRODUCTION

Operational Amplifier (OPA) models can be roughly categorized into a) Controlled Source (CS) models, b) white box macro models and c) Nullor models .

In CS models (see [1]), the power supplies are lumped within the OPA and controlled sources can provide an infinite amount of power. It has the advantage of being simple and hides most of the internal complexity. This is the method of choice used by students to study the functional behaviour of OPA circuits. The main drawback comes from the absence of external supply ports. This results in non passive models, and forbids simulations with non-ideal voltage sources (e.g. in low-budget guitar stomboxes).

White box macro models (see references [2] [3] [4]) use dozens of transistors to accurately reproduce the inner structure and non-ideal characteristics of particular devices. While this is appropriate for offline simulation and circuit design, the main drawback of this approach comes from the high number of (implicit) nonlinear equations which makes it often unsuitable for real-time simulation.

Nullors (see references [5] [6] [7] [8]), are singular two-port elements where the input flow and effort variables are both zero: $e_1 = f_1 = 0$, while the output flow and effort variables e_2, f_2 are unconstrained. One drawback is the lack of flow / effort duality. In addition, similar to CS, Nullors have no explicit power supply ports and thus are not passive devices, inheriting the same drawbacks mentioned above.

For audio applications, dedicated Wave Digital Filters (WDF) models of the OPA for specific circuit topologies have been proposed in [9], more recently, using Modified Nodal Analysis to WDF adaptors, both Nullor and CS general purpose models of the OPA and OTA have been proposed in [10] [11] and Sallen-key filters have been modelled with WDF in [12].

We propose a passive, quasi-ideal, black-box, behavioural model of the OPA, simple enough for realtime simulation, with explicit power supply and modelling nonlinear saturation. In particular, a by-product of this research is to have a model compatible with the port-Hamiltonian formalism [13].

The paper is structured as follows. First a general purpose passive model of the OPA is proposed in section 2, then it is illustrated by treating the non-inverting voltage amplifier circuit in section 3, finally a detailed study and simulation of a saturating Sallen-Key lowpass filter is presented in section 4.

2. OPERATIONAL AMPLIFIER MODEL

The objective of this paper is to find the simplest class of Operational Amplifier models satisfying the following properties:

a) Memoryless: infinite bandwidth, infinite slew rate,

b) Passivity: the power dissipated by the OPA is non-negative (i.e. hidden sources of energy are forbidden),

c) Quasi-ideal behaviour: infinite input impedance, zero output impedance, infinite common-mode rejection ratio,

d) Finite output voltage range and saturation: explicit non-constant power-supply ports,

e) Minimal: behavioural model with a minimum number of equations (i.e. not a white box model containing dozen of transistors).

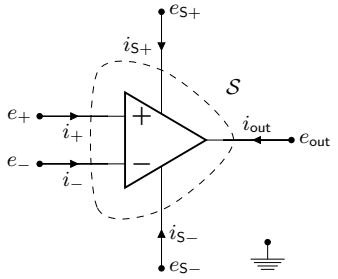

Figure 1: Circuit diagram of an Operational Amplifier (OPA) with currents drawn in receiver convention. The gaussian surface $\mathcal{S}$ enclosing the component is shown in dashed line.

* The author acknowledges the support of the ANR-DFG (French-German) project INFIDHEM ANR-16-CE92-0028.

2.1. Notations

The OPA shown on figure 1 is modelled as a 5-port device with node voltages being measured relatively to the ground, node currents directed toward the element using the receiver convention and pins labelled $\mathcal{P} = \{+, -, \mathsf{S}+, \mathsf{S}-, \mathsf{out}\}$. In this paper, we assume that the ports of the OPA can be partitioned into a voltage-driven set $\mathcal{T}$, and a current-controlled co-set $\mathcal{T}^*$

$$\mathcal{T} := \{+, -, \mathsf{S}+, \mathsf{S}-\}, \quad \mathcal{T}^* := \{\mathsf{out}\}, \quad \mathcal{T} \cup \mathcal{T}^* = \mathcal{P}. \tag{1}$$

The respective inputs and outputs are collected into the vectors

$$\mathbf{u} := [\mathbf{e}_{\mathcal{T}}, \mathbf{i}_{\mathcal{T}^*}]^{\mathsf{T}} = [e_+, e_-, e_{\mathsf{S}+}, e_{\mathsf{S}-}, i_{\mathsf{out}}]^{\mathsf{T}}, \tag{2}$$

$$\mathbf{y} := [\mathbf{i}_{\mathcal{T}}, \mathbf{e}_{\mathcal{T}^*}]^{\mathsf{T}} = [i_+, i_-, i_{\mathsf{S}+}, i_{\mathsf{S}-}, e_{\mathsf{out}}]^{\mathsf{T}}, \tag{3}$$

Finally, the common supply, the differential supply and the differential input voltages are respectively defined by

$$V_{\mathsf{cm}} = \frac{e_{\mathsf{S}+} + e_{\mathsf{S}-}}{2}, \quad V_{\mathsf{dm}} = \frac{e_{\mathsf{S}+} - e_{\mathsf{S}-}}{2}, \quad \epsilon = e_+ - e_-. \tag{4}$$

2.2. Constitutive equations

Since there are 5 ports with dual flow and efforts variables, 5 independent equations are required to specify the device:

1-2) **Non-energetic input ports**: the current entering the pins $\{+, -\}$ is zero (infinite input impedance)

$$i_+ = i_- = 0, \tag{5}$$

3) **Conservation of charge**: Kirchoff Current Law applied over the gaussian surface[1] $\mathcal{S}$ enclosing the AOP implies that the sum of all currents is zero

$$\sum_{\ell \in \mathcal{P}} i_\ell = 0, \tag{6}$$

4) **Passivity**: the power absorbed by the OPA is greater or equal to zero

$$P_{\mathsf{diss}} = \mathbf{y}^{\mathsf{T}}\mathbf{u} = \sum_{\ell \in \mathcal{P}} e_\ell \cdot i_\ell \geq 0, \tag{7}$$

5) **Differential gain and saturation**: the tensions are tied by a continuous relation $e_{\mathsf{out}} = f(e_+, e_-, e_{\mathsf{S}+}, e_{\mathsf{S}-})$ such that

$$\begin{cases} \dfrac{\partial f}{\partial \epsilon} \geq 0, & \text{monotonicity} \\ \max\left(\dfrac{\partial f}{\partial \epsilon}\right) = K, & \text{differential gain} \\ \max(f) = e_{\mathsf{S}+}, \ \epsilon \to +\infty & \text{positive saturation} \\ \min(f) = e_{\mathsf{S}-}, \ \epsilon \to -\infty & \text{negative saturation} \end{cases} \tag{8}$$

This gives 4 equalities and 1 inequality

$$i_+ = 0 \tag{9}$$

$$i_- = 0 \tag{10}$$

$$i_{\mathsf{S}+} + i_{\mathsf{S}-} + i_{\mathsf{out}} = 0 \tag{11}$$

$$P_{\mathsf{diss}} = i_{\mathsf{S}+} \cdot e_{\mathsf{S}+} + i_{\mathsf{S}-} \cdot e_{\mathsf{S}-} + i_{\mathsf{out}} \cdot e_{\mathsf{out}} \geq 0 \tag{12}$$

$$f(e_{\mathsf{S}+}, e_{\mathsf{S}-}, e_+, e_-) - e_{\mathsf{out}} = 0 \tag{13}$$

Since there is an inequality and the relation f is not specified yet, there is an infinite class of models satisfying these equations. A particular instance is chosen as follows.

[1] The Gaussian surface $\mathcal{S}$ is shown on figure 1. For more details see [1].

2.3. Toward a unique model

Substituting (4) into the passivity equation (12), using the conservation of charge (11) and simplifying by i_{out} gives the constraint[2]

$$V_{\mathsf{cm}} + V_{\mathsf{dm}} \left(\frac{i_{\mathsf{S}+} - i_{\mathsf{S}-}}{i_{\mathsf{S}+} + i_{\mathsf{S}-}} \right) = e_{\mathsf{out}} - \frac{P_{\mathsf{diss}}}{i_{\mathsf{out}}}, \quad (i_{\mathsf{out}} \neq 0) \tag{14}$$

which imposes a lot of structure on the form of the output function. In order to specify a unique model, the following choices are made.

2.3.1. Differential input transistor pair

First, motivated by the typical structure of an OPA, composed of a differential pair of transistors, gain stages and a push-pull output (see [14] p.707), the adimensioned modulation factor [3]

$$\rho(\epsilon) := -\frac{i_{\mathsf{S}+}}{i_{\mathsf{out}}} = \frac{\exp(x)}{\exp(x) + \exp(-x)}, \quad x = \frac{K\epsilon}{V_{\mathsf{dm}}}, \tag{15}$$

is introduced and shown on figure 2. According to the conservation of charge (11), this leads to the symmetric current splitting

$$i_{\mathsf{S}+} = -\rho(\epsilon) i_{\mathsf{out}}, \qquad i_{\mathsf{S}-} = -\rho(-\epsilon) i_{\mathsf{out}}. \tag{16}$$

2.3.2. The conservative OPA choice

Second, among all passive OPA models, the conservative ones are chosen, neglecting internal dissipation:

$$P_{\mathsf{diss}} = 0. \tag{17}$$

The power supply ports provide the amount of power necessary to balance the power consumed at the output port. This is an instance of a nonlinear nonenergic n-port [15].

2.3.3. Final model

Substituting (16) and (17) into (14) uniquely defines the output function (a similar result was also derived in [16])

$$e_{\mathsf{out}} = V_{\mathsf{cm}} + V_{\mathsf{dm}} \tanh\left(\frac{K\epsilon}{V_{\mathsf{dm}}}\right). \tag{18}$$

Expressed as a function of $e_{\mathsf{S}+}, e_{\mathsf{S}-}$ this gives

$$e_{\mathsf{out}} = \rho(+\epsilon) e_{\mathsf{S}+} \ + \ \rho(-\epsilon) e_{\mathsf{S}-}. \tag{19}$$

Finally gathering equations (5) (16) (19) in matrix form reveals the modulated hybrid Dirac structure[4] of the conservative OPA model given by the skew-symmetric matrix $\mathbf{J}(\mathbf{u})$:

$$\underbrace{\begin{bmatrix} i_+ \\ i_- \\ i_{\mathsf{S}+} \\ i_{\mathsf{S}-} \\ e_{\mathsf{out}} \end{bmatrix}}_{\mathbf{y}} = \underbrace{\left[\begin{array}{cc|ccc} . & . & . & . & . \\ . & . & . & . & . \\ \hline . & . & . & . & -\rho(+\epsilon) \\ . & . & . & . & -\rho(-\epsilon) \\ . & . & \rho(\epsilon) & \rho(-\epsilon) & . \end{array}\right]}_{\mathbf{J}(\mathbf{u})} \underbrace{\begin{bmatrix} e_+ \\ e_- \\ e_{\mathsf{S}+} \\ e_{\mathsf{S}-} \\ i_{\mathsf{out}} \end{bmatrix}}_{\mathbf{u}}. \tag{20}$$

The singularity of the structure matrix $\mathbf{J}$ encodes the conservation of the so-called Casimir invariants $i_+ = i_- = 0$, in addition to the conservative power-balance

$$P_{\mathsf{diss}} = \mathbf{u}^{\mathsf{T}}\mathbf{y} = \mathbf{u}^{\mathsf{T}}\mathbf{J}(\mathbf{u})\mathbf{u} = 0, \quad (\mathbf{J} = -\mathbf{J}^{\mathsf{T}}). \tag{21}$$

[2] see appendix A for a detailed proof.

[3] Different choices can be made here to adapt to other transistors types.

[4] Please refer to the references [17] [18] [13] for more details on Dirac structures and to [1] for hybrid parameters.

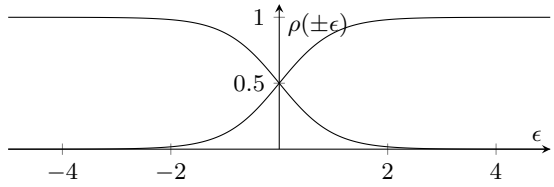

Figure 2: The modulation factor $\rho(\pm\epsilon)$, for $K = 1$, $V_{\mathsf{dm}} = 1$.

3. CASE STUDY

To study the behaviour of the proposed model in practical applications, the case of the voltage amplifier is examined in section 3.1. Then as a pedagogical example, the voltage amplifier is driven by a sinusoidal voltage source and asymmetrically powered by a single capacitor to simulate a discharging battery in section 3.2. The voltage amplifier will be used as a building block of the Sallen-Key lowpass filter shown in section 4.

3.1. The non-inverting voltage amplifier

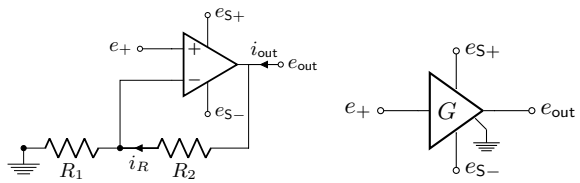

(a) (b)

Figure 3: a) a non-inverting voltage amplifier circuit with explicit alimentation ports and b) its symbol.

A non-inverting voltage amplifier (figure 3) is achieved by feeding back the output e_{out} to the negative input e_- through a voltage divider

$$\epsilon = e_+ - \frac{e_{\mathsf{out}}}{G}, \qquad G = \frac{R_1 + R_2}{R_1} = 1 + \frac{R_2}{R_1}. \tag{22}$$

The instantaneous feedback makes the circuit act as a proportional corrector with high proportional gain K in order to satisfy the constraint $e_{\mathsf{out}} \approx G e_+$ within the range $e_{\mathsf{out}} \in [e_{\mathsf{S}+}, e_{\mathsf{S}-}]$.

The voltage divider induces an internal current $i_R = e_{\mathsf{out}}/R$, where $R = R_1 + R_2$, and the current splitting (16) becomes

$$i_{\mathsf{S}+} = -\rho(\epsilon)(i_{\mathsf{out}} - i_R), \quad i_{\mathsf{S}-} = -\rho(-\epsilon)(i_{\mathsf{out}} - i_R). \tag{23}$$

This results in the following law for the voltage amplifier

$$\begin{bmatrix} i_+ \\ i_{\mathsf{S}+} \\ i_{\mathsf{S}-} \\ e_{\mathsf{out}} \end{bmatrix} = \left[\begin{array}{c|cc|c} . & . & . & . \\ \hline . & g_+(\epsilon) & g_\pm(\epsilon) & -\rho(\epsilon) \\ . & g_\pm(\epsilon) & g_-(\epsilon) & -\rho(-\epsilon) \\ \hline . & \rho(\epsilon) & \rho(-\epsilon) & . \end{array}\right] \begin{bmatrix} e_+ \\ e_{\mathsf{S}+} \\ e_{\mathsf{S}-} \\ i_{\mathsf{out}} \end{bmatrix}. \tag{24}$$

with conductances

$$g_+(\epsilon) = \frac{\rho(\epsilon)^2}{R}, \; g_-(\epsilon) = \frac{\rho(-\epsilon)^2}{R}, \; g_\pm(\epsilon) = \frac{\rho(\epsilon)\rho(-\epsilon)}{R}. \tag{25}$$

In the following, it is assumed that $R \to \infty$ such that internal losses are negligible. In particular, this is the case of the classical voltage follower circuit for which $R_2 = 0$, and $R_1 = \infty$.

3.1.1. Implicit constraint

The relation (24) is still implicitly defined since ϵ depends on both input and output variables e_+ and e_{out}. To avoid apparent difficulties with discontinuous functions, consider the curve

$$\mathcal{F} = \left\{ (u, y) \in \mathbb{R}^2 \mid F(u, y) = 0 \right\}, \tag{26}$$

specified by the function

$$F(u, y) = V_{\mathsf{cm}} + V_{\mathsf{dm}} \tanh\left(\frac{K}{V_{\mathsf{dm}}} \left(u - \frac{y}{G} \right) \right) - y, \tag{27}$$

and given e_+, look for e_{out} such that $(e_+, e_{\mathsf{out}}) \in \mathcal{F}$.

Since the output function is monotonous with respect to ϵ and bounded in $[e_{\mathsf{S}-}, e_{\mathsf{S}+}]$, a unique solution exists within that range. A global method such as the bisection method is guaranteed to find it, whereas, since K is typically about 10^6, it is very difficult to use either fixed-point or derivative-based methods because of bad numerical conditioning. Numerical simulations are shown on figure 4.

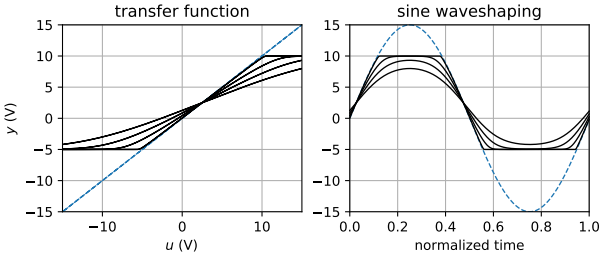

Figure 4: Transfer function of the voltage amplifier for $G = 1$, $K \in \{1, 2, 5, 50\}$, $e_{\mathsf{S}+} = 10\text{V}$, $e_{\mathsf{S}-} = -5\text{V}$. Smaller values than the typical OPA gain $K \approx 10^6$ are used for visualisation purposes.

3.1.2. Explicit representation

Taking the limit when $K \to \infty$ gives an explicit representation of $\mathcal{F}$ as the piecewise continuous curve

$$\mathcal{F}_\infty = \lim_{K\to\infty} \mathcal{F} : \begin{cases} y = e_{\mathsf{S}+}, & Gu > y \\ y = e_{\mathsf{S}-}, & Gu < y \\ y \in [e_{\mathsf{S}-}, e_{\mathsf{S}+}], & y = Gu \end{cases}. \tag{28}$$

One can see on figure 4 that convergence to $\mathcal{F}_\infty$ is very fast even for moderate values of K. This justifies the use of this limit process in following developments.

For $(e_+, e_{\mathsf{out}}) \in \mathcal{F}_\infty$ this gives the explicit form

$$e_{\mathsf{out}} = V_{\mathsf{cm}} + V_{\mathsf{dm}} \operatorname{sat}\left(\frac{G e_+ - V_{\mathsf{cm}}}{V_{\mathsf{dm}}} \right), \tag{29}$$

where

$$\operatorname{sat}(x) = \min(\max(x, -1), 1). \tag{30}$$

Alternatively one can represent this function as

$$e_{\mathsf{out}} = \mu_+(e_+, V_{\mathsf{cm}}, V_{\mathsf{dm}}) e_{\mathsf{S}+} + \mu_-(e_+, V_{\mathsf{cm}}, V_{\mathsf{dm}}) e_{\mathsf{S}-} \tag{31}$$

where the implicit modulation factor $\rho(\pm\epsilon)$ in (24) has been replaced by the explicit one

$$\mu_\pm(e_+, V_{\mathsf{cm}}, V_{\mathsf{dm}}) = \frac{1 \pm \operatorname{sat}(x)}{2}, \quad x = \frac{G e_+ - V_{\mathsf{cm}}}{V_{\mathsf{dm}}}. \tag{32}$$

3.2. A single-rail voltage follower powered by a capacitor

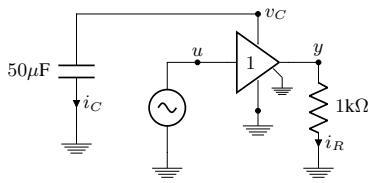

Figure 5: A single-rail voltage amplifier powered by a capacitor.

To illustrate one of the practical interest of having explicit power supply ports, the voltage amplifier is used with the negative supply port grounded, and the positive supply port powered by a capacitor to simulate a discharging battery (figure 5).

Using (20) with $V_{\text{cm}} = V_{\text{dm}} = q/(2C)$, and $i_{\text{out}} = -y/R$, yields the algebro-differential equations

$$\begin{cases} \dot{q} = -\eta(u,q)\dfrac{y}{R}, \\ y = \eta(u,q)\dfrac{q}{C} \end{cases}, \quad \eta(u,q) = \mu_+\left(u, \frac{q}{2C}, \frac{q}{2C}\right). \tag{33}$$

The energy stored in the capacitor is $H(q) = q^2/2C$. Then its differential equation is governed by the monotonous discharge

$$\frac{\mathrm{d}}{\mathrm{d}t}H(q) = \frac{\partial H}{\partial q}\frac{\mathrm{d}q}{\mathrm{d}t} = -\frac{q}{C}\eta(q,u)\frac{y}{R} = -\frac{y^2}{R}. \tag{34}$$

The circuit acts as a half-wave rectifier with a positive clipping threshold governed by the discharge of the capacitor as shown on figure 6.

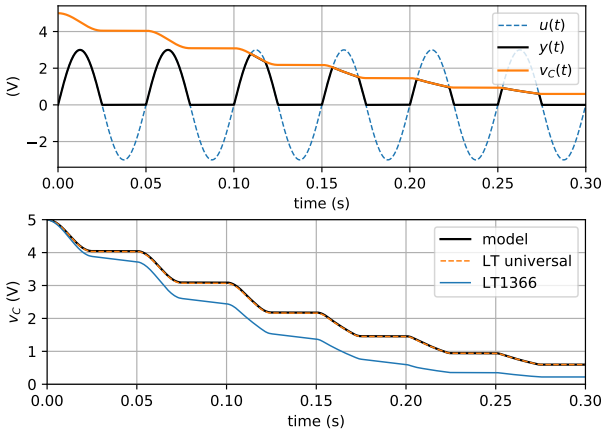

Figure 6: Time domain simulation of the capacitor-powered single rail voltage amplifier with $v_C(0) = 5\text{V}$ and $|u| = 3V$. Top plot: proposed model. Bottom plot: comparison of discharge rate with LTspice's Universal OPA level.2 and the LT1366 [19].

Remark (Comparison between models)

As expected, with the proposed model, the capacitor does not discharge during negative saturation (energy-preservation), and has a monotonous discharge otherwise. Comparison with LTspice's universal model shows that the two simulations are very close. Finally with the LT1366, the discharge is monotonous and qualitatively similar, but decays faster due to internal dissipation.

4. SALLEN-KEY ANALOG LOWPASS FILTER

The class of Sallen-Key Filters (SKF), introduced in [20], is perhaps one of the most common analog filter design topology. It is used for the realization of analog biquadratic filters, for example in parametric equalisers. It is also the basis of the multimode Steiner filter [21], the Korg MS-20 [22] and the Buchla Lowpass-Gate [23].

A Sallen-Key lowpass filter schematic is shown on figure 8a. The linear regime and its control parameters are studied in 4.1, the circuit is then converted into equations in 4.2. Discretization is performed using the Average Vector Field method in 4.3, finally simulation results are shown in 4.4.

4.1. Linear behaviour and control parameters

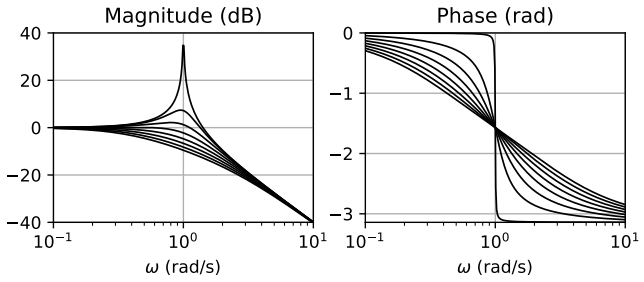

Figure 7: Bode plot of the Sallen-Key filter for $\omega = 1$, $G \in [0, 3]$

It is recalled that the Laplace transfer function (shown on figure 7) of a second order resonant lowpass filters with pulsation ω and quality factor Q is

$$H_{\text{LP}}(s) = \frac{1}{1 + \frac{1}{Q}\left(\frac{s}{\omega}\right) + \left(\frac{s}{\omega}\right)^2}, \tag{35}$$

In the linear regime, the Laplace transfer function of the lowpass Sallen-Key filter is

$$H_{\text{SK}}(s) = \mathcal{L}\left\{\frac{y_{\text{SK}}}{v_{\text{IN}}}\right\} = \frac{1}{1 + a_1 s + a_2 s^2}, \tag{36}$$

where

$$a_1 = \big((1-G)R_1C_1 + (R_1 + R_2)C_2\big), \tag{37}$$

$$a_2 = C_1C_2R_1R_2. \tag{38}$$

Since there are only two target controls (ω, Q), for 5 design parameters (R_1, R_2, C_1, C_2, G), there are many possible design decisions that are often decided according to electronic constraints.

In this paper, the Steiner filter parametrization is used with $R_1 = R_2 = R$, and $C_1 = C_2 = C$ because of its simplicity. The transfer function (36) simplifies to

$$H_{\text{SK}}(s) = \frac{1}{1 + (3-G)\left(\frac{s}{\omega}\right) + \left(\frac{s}{\omega}\right)^2}, \tag{39}$$

with $\omega = 1/(RC)$, and $Q = 1/(3-G)$. In simulations, capacitances are both set to $C = 4.7\text{nF}$ and the resistors are adjusted to achieve the target cutoff frequencies.

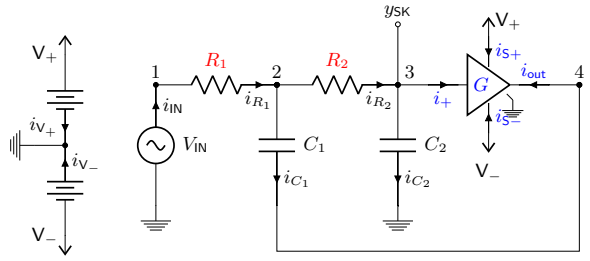

(a) Circuit

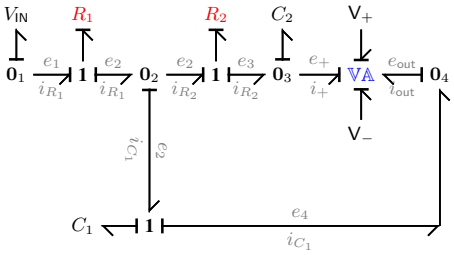

(b) Bondgraph

	V_{IN}	v_{C_1}	v_{C_2}	V_+	V_-	i_{R_1}	i_{R_2}	i_+	i_{S+}	i_{S-}	e_{out}
i_{IN}						−1	.	.	.	.	
i_{C_1}						1	−1	.	.	.	
i_{C_2}						.	1	−1	.	.	
i_{V_+}						.	.	.	−1	.	
i_{V_-}						.	.	.	.	−1	
v_{R_1}	1	−1	.	.	.						−1
v_{R_2}	.	1	−1	.	.						1
e_+	.	.	1	.	.						.
e_{S+}	.	.	.	1	.						.
e_{S-}	.	.	.	.	1						.
i_{out}						1	−1	.	.	.	

(c) Skew-symmetric Dirac structure (KCL+KVL)

$$\begin{pmatrix} i_{C_1} \\ i_{C_2} \\ \hline i_{IN} \\ i_{out} \end{pmatrix} = \underbrace{\frac{1}{R}\left(\begin{array}{cc|cc} -2 & 1 & 1 & -2 \\ 1 & -1 & 0 & 1 \\ \hline 1 & 0 & -1 & 1 \\ -2 & 1 & 1 & -2 \end{array}\right)}_{Y} \begin{pmatrix} v_{C_1} \\ v_{C_2} \\ \hline v_{IN} \\ e_{out} \end{pmatrix}$$

(d) Reduced model (admittance form)

Figure 8: a) The original Sallen-Key lowpass filter circuit, b) its corresponding bondgraph (see references [24] [25] [26]) with computational causality assignment. c) the skew-symmetric Dirac structure representing Kirchoff conservation laws. d) the reduced dynamical model.

4.2. Modelling

To model the Sallen-Key filter, the following systematic approach is used:

- **Bondgraph**: The circuit 8a is first converted to an equivalent bondgraph 8b using the rules in [25]. A bond between two ports **A** ⟶ **B** stands for a pair of dual port-variables (e, f). The half-arrow indicates the power sign convention $P = ef \geq 0$. **0** denotes a parallel junction where all bonds share the same voltage, and **1** denotes a serial junction where all bonds share the same current.
- **Causality assignment**: to convert an acausal bidirectional bondgraph to a causal, computable, block-diagram, one needs to partition the flows and efforts into inputs and outputs. The convention uses a vertical stroke **A** ⟼ **B** next to ports that are effort-controlled. *Computational causalities* can be assigned graphically by propagating the following rules: voltage sources and capacitors have an effort-out causality, **0** junctions can only have one input effort, while the dual **1** junctions can only have one output effort.
- **Dirac Structure**: given the causality assignment, shown on 8b, into inputs and outputs, it is now straightforward to fill the Dirac Structure matrix 8c by inspecting circuit 8a and expressing Kirchoff's current and voltage laws.
- **Reduced model**: one can reduce the model by solving trivial equalities like $e_+ = v_{C_2}$, $e_{S+} = V_+$, $e_{S-} = V_-$, treating $V_\pm$ as constants and replacing the linear resistive currents (i_{R_1}, i_{R_2}) by their constitutive laws. This results in the reduced admittance model shown on figure 8d.

4.2.1. *Nonlinear feedback*

To separate the linear and nonlinear feedback, one can write

$$\hat{e}_{out}(v) = Gv - \nabla N(v) \tag{40}$$

where the nonlinear law is

$$\begin{aligned} \nabla N(v) &:= Gv - \hat{e}_{out}(v) \\ &= \min(0, Gv - e_{S-}) + \max(0, Gv - e_{S+}). \end{aligned} \tag{41}$$

and its algebraic potential (figure 9) is given by the line integral

$$\begin{aligned} N(v) &:= \int_0^v \nabla N(s) \cdot \mathrm{d}s \\ &= \frac{\min(0, Gv - e_{S-})^2}{2G} + \frac{\max(0, Gv - e_{S+})^2}{2G}. \end{aligned} \tag{42}$$

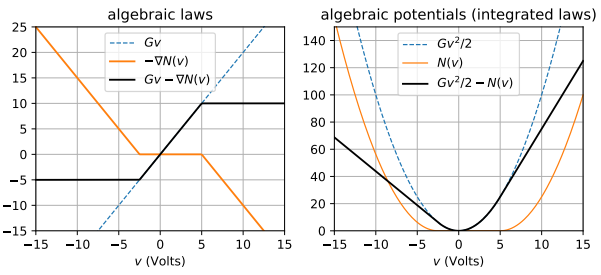

Figure 9: Algebraic feedback laws and their potentials shown for $G = 2$, $e_{S+} = 10\text{V}$, $e_{S-} = -5\text{V}$.

4.2.2. State-space model

Finally replacing the flow and effort variables by their constitutive laws, and only considering the input-state-output, one gets

$$\begin{cases} \dot{\mathbf{x}} = \omega \left[\mathbf{A}\mathbf{x} + \mathbf{B}\mathbf{u} - \mathbf{F}\nabla N(\mathbf{C}\mathbf{x}) \right] \\ \mathbf{y} = \mathbf{C}\mathbf{x} \end{cases}, \tag{43}$$

where $\mathbf{u} = v_{\mathsf{IN}}$, $\mathbf{y} = y_{\mathsf{SK}}$, $\mathbf{x} = [v_{C_1}, v_{C_2}]^{\mathsf{T}}$, $\omega = 1/(RC)$ and

$$\mathbf{A} = \begin{bmatrix} -2 & 1-2G \\ 1 & -1+G \end{bmatrix}, \qquad \mathbf{B} = \begin{bmatrix} 1 \\ 0 \end{bmatrix}, \tag{44}$$

$$\mathbf{C} = \begin{bmatrix} 0 & 1 \end{bmatrix}, \qquad \mathbf{F} = \begin{bmatrix} -2 \\ 1 \end{bmatrix}. \tag{45}$$

Using the co-energy variables v_{C_1}, v_{C_2} instead of the energy variables q_{C_1}, q_{C_2} is justified here by the fact that the capacitors are linear and time-invariant, i.e. the co-energy $H^*(v) = Cv^2/2$ equals the energy $H(q) = q^2/(2C)$ for the linear law $v = q/C$.

4.3. Discretization using the AVF method

The Average Vector Field (AVF) method is used to discretize (43) because of its structure-preserving properties: it preserves the energy (resp. dissipativity) of conservative (resp. dissipative) systems (see [27]). One can also refer to [28] where it has been shown that the bilinear transform doesn't always guarantee the dissipativity of nonlinear filters (whether time-varying or not).

As an important side-effect, the AVF method can also be interpreted as a first-order instance of anti-derivative antialiasing [29].

4.3.1. The Average Vector Field method

Let $\Omega = [t_0, t_0 + h]$ be a time-step, $\mathbf{x} : \Omega \to \mathbb{R}^n$ a locally affine trajectory parametrized by the normalized variable $\tau \in [0, 1]$

$$\mathbf{x}(t_0 + h\tau) = \mathbf{x}_0 + \tau(\mathbf{x}_1 - \mathbf{x}_0). \tag{46}$$

Introduce the averaging operator $\mathcal{A}$, defined for all functions $f : \mathbb{R}^n \to \mathbb{R}^n$ or operators $f : \mathcal{H} \to \mathcal{H}$, where $\mathcal{H}$ is a functional space from $\Omega \to \mathbb{R}^n$, by

$$(\mathcal{A}\, f)(\mathbf{x}) := \int_0^1 f(\mathbf{x}(t_0 + h\tau))\, \mathrm{d}\tau. \tag{47}$$

For the time derivative and identity operators, one gets

$$\overline{\dot{\mathbf{x}}} := \left(\mathcal{A} \tfrac{\mathrm{d}}{\mathrm{d}t} \right) \mathbf{x} = \frac{\mathbf{x}_1 - \mathbf{x}_0}{h}, \quad \bar{\mathbf{x}} := (\mathcal{A}\mathcal{I})\mathbf{x} = \frac{\mathbf{x}_0 + \mathbf{x}_1}{2}. \tag{48}$$

Using the gradient theorem, this gives the average discrete gradient

$$\begin{aligned} \overline{\nabla} N(v_0, v_1) &:= (\mathcal{A}\nabla N)(v_0 + \tau(v_1 - v_0)) \\ &= \begin{cases} \dfrac{N(v_1) - N(v_0)}{v_1 - v_0} & v_0 \neq v_1 \\ \nabla N(v_0) & v_0 = v_1 \end{cases}. \end{aligned} \tag{49}$$

Computing its derivative with respect to v_1 leads to

$$\frac{\partial \overline{\nabla} N}{\partial v_1}(v_0, v_1) = \begin{cases} \dfrac{\nabla N(v_1) - \overline{\nabla} N(v_0, v_1)}{v_1 - v_0} & v_0 \neq v_1 \\ \dfrac{1}{2}\nabla^2 N(v_0) & v_0 = v_1 \end{cases}. \tag{50}$$

One can refer to [30], where the discrete gradient's derivative is also used for numerical simulation.

4.3.2. Averaged system

Applying the averaging operator $\mathcal{A}$ to (43), leads to the structure-preserving discrete algebraic system

$$\begin{cases} \overline{\dot{\mathbf{x}}} = \omega \left[\mathbf{A}\bar{\mathbf{x}} + \mathbf{B}\bar{\mathbf{u}} - \mathbf{F}\, \overline{\nabla} N(\mathbf{C}\mathbf{x}_0, \mathbf{C}\mathbf{x}_1) \right] \\ \bar{\mathbf{y}} = \mathbf{C}\bar{\mathbf{x}} \end{cases}. \tag{51}$$

Solving the linear part for $\mathbf{x}_1$ gives the discrete state-space update

$$\mathbf{x}_1 = \mathbf{A}_d\mathbf{x}_0 + \mathbf{B}_d\bar{\mathbf{u}} - \mathbf{F}_d\, \overline{\nabla} N(\mathbf{C}\mathbf{x}_0, \mathbf{C}\mathbf{x}_1), \tag{52}$$

with the normalised pulsation $\omega_d = h\omega$ and

$$\begin{aligned} \mathbf{A}_d &= \mathbf{D}^{-1}\left(\mathbf{I} + \frac{\omega_d}{2}\mathbf{A} \right), & \mathbf{B}_d &= \mathbf{D}^{-1}(\omega_d \mathbf{B}), \\ \mathbf{D} &= \left(\mathbf{I} - \frac{\omega_d}{2}\mathbf{A} \right), & \mathbf{F}_d &= \mathbf{D}^{-1}(\omega_d \mathbf{F}). \end{aligned} \tag{53}$$

4.4. Simulation

Simulation results[5] are shown on figures 10 and 11 and exhibit a very close match with offline simulations performed in LTspice. To solve (52), one can either use the simple fixed-point iteration, or Newton's method.

4.4.1. Fixed-point iteration

A simple numerical scheme is to look for the fixed-point $\mathbf{x}_1 = \phi(\mathbf{x}_1)$ of the pre-conditioned fixed-point function

$$\phi(\mathbf{x}_1) := \mathbf{A}_d\mathbf{x}_0 + \mathbf{B}_d\bar{\mathbf{u}} - \mathbf{F}_d\, \overline{\nabla} N(\mathbf{C}\mathbf{x}_0, \mathbf{C}\mathbf{x}_1), \tag{54}$$

with the fixed-point iteration

$$\mathbf{x}_1^{k+1} = \phi\left(\mathbf{x}_1^k \right), \quad \mathbf{x}_1^0 = \mathbf{x}_0. \tag{55}$$

A sufficient convergence condition is detailed in appendix B.

In practice, thanks to the non linear feedback splitting in (40), when the OPA is in the linear regime, $\nabla N = 0$. Then the iteration reduces to an explicit one-step trapezoidal integrator and converges in only one iteration.

4.4.2. Newton iteration

To accelerate convergence, one can use Newton's method [31] as follows: define the auxiliary function

$$\varphi(\mathbf{x}_1) = \mathbf{x}_1 - \phi(\mathbf{x}_1), \tag{56}$$

and look for the root $\mathbf{x}_1^*$ such that $\varphi(\mathbf{x}_1^*) = 0$ with the Newton iteration

$$\mathbf{x}_1^{k+1} = \mathbf{x}_1^k - \left(\varphi'(\mathbf{x}_1^k) \right)^{-1} \varphi(\mathbf{x}_1^k), \quad \mathbf{x}_1^0 = \mathbf{x}_0. \tag{57}$$

where the Jacobian of φ is given by

$$\varphi'(\mathbf{x}_1) = \mathbf{I} + \mathbf{F}_d\mathbf{C}\, \frac{\partial \overline{\nabla} N}{\partial v_1}(\mathbf{C}\mathbf{x}_0, \mathbf{C}\mathbf{x}_1). \tag{58}$$

[5] Sound examples and LTspice files are available at the accompanying website: `https://github.com/remymuller/dafx19-opa`.

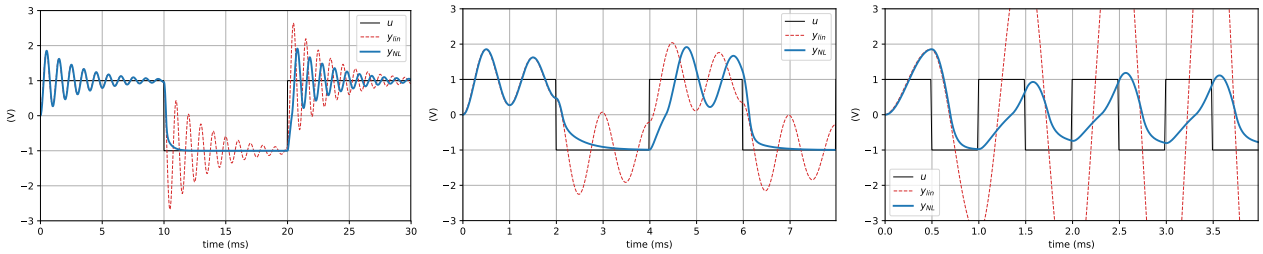

(a) $f_0 = 50$Hz (b) $f_0 = 250$Hz (c) $f_0 = 1$kHz

Figure 10: SKF filter response to a square wave input with sampling frequency $f_s = 44.1$kHz, $C = 4.7$nF, cutoff $f_c = 1$kHz ($R = 33.8k\Omega$), $Q = 10$, asymmetric saturation $V_+ = 15$V, $V_- = 0$V and different fundamental frequencies. The non linear SKF response is shown in solid blue, with the linear SKF response in dashed red for reference.

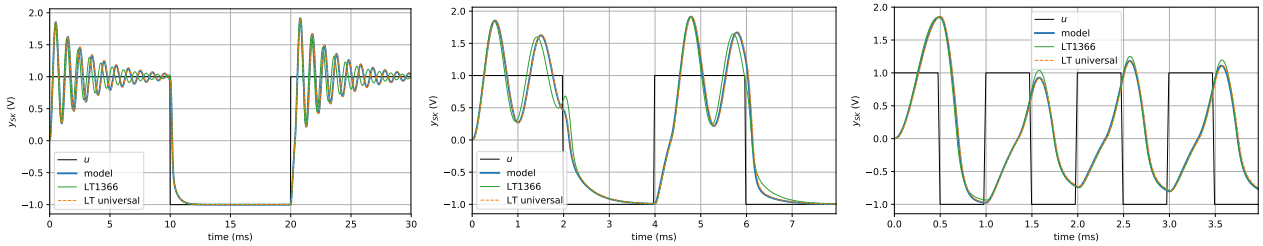

(a) $f_0 = 50$Hz (b) $f_0 = 250$Hz (c) $f_0 = 1$kHz

Figure 11: Comparison between the proposed model, LTspice's universal OPA level.2 and the LT1366 opamp. The proposed model output is almost indistinguishable from LTspice's universal model, whereas the tuning of the LT1366 is slightly different because of dissipation.

5. CONCLUSIONS AND PERSPECTIVES

In this paper, a static, passive, black-box model of the operational amplifier with explicit power supply has been examined. It is suitable for the modelling of audio circuits and simple enough for real-time simulation. Furthermore the explicit modelling of external power supply ports allows the use of non-ideal voltage sources.

The choice has been made to ignore internal dissipation to keep the model minimal. However, non-ideal characteristics such as input and output impedance or power supply voltage drop can be achieved by modular composition of the model with other circuit elements. This will be the topic of further research.

The non inverting amplifier is also derived as a dedicated building block. Numerical simulations justify the use of an infinite OPA gain to get an explicit formulation. Having a pre-solved amplifier model also greatly simplifies its use in electronic circuits, avoiding numerical stiffness and high index DAE.

Finally, the amplifier is used for audio simulations to model a saturating Sallen-Key lowpass filter of second order. A reduced state-space model is derived from the circuit schematic, and a structure-preserving discretization is performed using the average vector field method. A comparison with LTspice shows that our results are very close to those of more complex macro models.

The perspectives of this study are a) modelling other non-ideal OPA characteristics such as finite slew-rate and bandwidth, current and voltage offsets, non-zero common-mode input gain. . . b) studying the behaviour of the model in other typical circuits (oscillator, rectifier, comparator) and c) experimental comparison with specific devices such as the common μA741, or TL072 audio OPAs.

6. REFERENCES

[1] L. O. Chua, C. A. Desoer, and E. S. Kuh, *Linear and nonlinear circuits*. McGraw-Hill College, 1987.

[2] G. R. Boyle, D. Pederson, B. Cohn, and J. E. Solomon, "Macromodeling of integrated circuit operational amplifiers," *IEEE Journal of Solid-State Circuits*, vol. 9, no. 6, pp. 353–364, 1974.

[3] B. Carter and T. R. Brown, *Handbook of operational amplifier applications*. Texas Instruments Dallas, Tex, USA, 2001.

[4] M. Alexander and D. F. Bowers, "Spice-compatible op amp macro-models," *Analog Devices, Application Note, AN-138*, 1990.

[5] H. Carlin, "Singular network elements," *IEEE Transactions on circuit theory*, vol. 11, no. 1, pp. 67–72, 1964.

[6] B. Tellegen, "On nullators and norators," *IEEE Transactions on circuit theory*, vol. 13, no. 4, pp. 466–469, 1966.

[7] L. Odess and H. Ur, "Nullor equivalent networks of non-ideal operational amplifiers and voltage-controlled sources," *IEEE Transactions on Circuits and Systems*, vol. 27, no. 3, pp. 231–235, 1980.

[8] G. Martinelli, "On the nullor," *Proceedings of the IEEE*, vol. 53, no. 3, pp. 332–332, 1965.

[9] R. C. Paiva, S. D'Angelo, J. Pakarinen, and V. Valimaki, "Emulation of operational amplifiers and diodes in audio distortion circuits," *IEEE Transactions on Circuits and Systems II: Express Briefs*, vol. 59, no. 10, pp. 688–692, 2012.

[10] K. J. Werner, W. R. Dunkel, M. Rest, M. J. Olsen, and J. O. Smith, "Wave digital filter modeling of circuits with operational amplifiers," in *2016 24th European Signal Processing Conference (EUSIPCO)*, pp. 1033–1037, IEEE, 2016.

[11] Ó. Bogason and K. J. Werner, "Modeling circuits with operational transconductance amplifiers using wave digital filters," in *Proc. 20th Int. Conf. Digital Audio Effects, Edinburgh, UK*, pp. 130–137, 2017.

[12] M. Verasani, A. Bernardini, and A. Sarti, "Modeling sallen-key audio filters in the wave digital domain," in *2017 IEEE International Conference on Acoustics, Speech and Signal Processing (ICASSP)*, pp. 431–435, IEEE, 2017.

[13] A. Schaft, "Port-hamiltonian systems: an introductory survey," 2006.

[14] A. S. Sedra and K. C. Smith, *Microelectronic circuits*. New York: Oxford University Press, 1998.

[15] J. L. Wyatt and L. Chua, "A theory of nonenergic n-ports," *International Journal of Circuit Theory and Applications*, vol. 5, no. 2, pp. 181–208, 1977.

[16] J. Mačák, *Real-time digital simulation of guitar amplifiers as audio effects*. PhD thesis, Brno University of Technology, Brno, 2012.

[17] T. J. Courant, "Dirac manifolds," *Transactions of the American Mathematical Society*, vol. 319, no. 2, pp. 631–661, 1990.

[18] A. J. Van Der Schaft, *L2-gain and passivity techniques in nonlinear control*, vol. 3. Springer, 2000.

[19] A. Devices, "Lt1366 datasheet." `https://www.analog.com/en/products/lt1366.html`, 2019. Online; accessed: 2019-03-22.

[20] R. P. Sallen and E. L. Key, "A practical method of designing rc active filters," *IRE Transactions on Circuit Theory*, vol. 2, no. 1, pp. 74–85, 1955.

[21] N.Steiner, "Voltage-tunable active filter features, low, high and bandpass modes," in *Electronic design 25, December 6*, 1974.

[22] T. Stinchcombe, "A study of the korg ms10 & ms20 filters." `http://www.timstinchcombe.co.uk/synth/MS20_study.pdf`, 2006. Online; accessed: 2019-03-22.

[23] J. Parker and S. D'Angelo, "A digital model of the buchla lowpass-gate," in *Proc. Int. Conf. Digital Audio Effects (DAFx-13), Maynooth, Ireland*, pp. 278–285, 2013.

[24] H. M. Paynter, *Analysis and design of engineering systems*. MIT press, 1961.

[25] P. C. Breedveld, "A systematic method to derive bond graph models," in *Second European Simulation Congress, Antwerp, Belgium*, 1986.

[26] J. F. Broenink, "Introduction to physical systems modelling with bond graphs," *SiE whitebook on simulation methodologies*, vol. 31, 1999.

[27] E. Celledoni, V. Grimm, R. I. McLachlan, D. McLaren, D. O'Neale, B. Owren, and G. Quispel, "Preserving energy resp. dissipation in numerical pdes using the average vector field method," *Journal of Computational Physics*, vol. 231, no. 20, pp. 6770–6789, 2012.

[28] T. Hélie, "Lyapunov stability analysis of the moog ladder filter and dissipativity aspects in numerical solutions," in *Proceedings of the 14th International Conference on Digital Audio Effects DAFx-11, Paris, France*, pp. 19–23, 2011.

[29] S. Bilbao, F. Esqueda, J. D. Parker, and V. Välimäki, "Antiderivative antialiasing for memoryless nonlinearities," *IEEE Signal Processing Letters*, vol. 24, no. 7, pp. 1049–1053, 2017.

[30] R. Muller and T. Hélie, "Power-balanced modelling of circuits as skew gradient systems," in *21 st International Conference on Digital Audio Effects (DAFx-18)*, 2018.

[31] P. Deuflhard, *Newton methods for nonlinear problems: affine invariance and adaptive algorithms*, vol. 35. Springer Science & Business Media, 2011.

A. STRUCTURE OF THE OUTPUT EQUATION

Using the passivity equation (12), then introducing $V_{\mathsf{cm}}, V_{\mathsf{dm}}$ using (4), factoring $V_{\mathsf{cm}}, V_{\mathsf{dm}}$, finally, for $i_{\mathsf{out}} \neq 0$, dividing by i_{out} and using (11) one gets the general form for the output equation (14).

Proof.

$$\begin{aligned}
& i_{\mathsf{S}+} \cdot e_{\mathsf{S}+} + i_{\mathsf{S}-} \cdot e_{\mathsf{S}-} = -i_{\mathsf{out}} \cdot e_{\mathsf{out}} - P_{\mathsf{diss}} \\
\iff\ & i_{\mathsf{S}+}(V_{\mathsf{cm}} + V_{\mathsf{dm}}) + i_{\mathsf{S}-}(V_{\mathsf{cm}} - V_{\mathsf{dm}}) = -i_{\mathsf{out}} \cdot e_{\mathsf{out}} - P_{\mathsf{diss}} \\
\iff\ & V_{\mathsf{cm}}(i_{\mathsf{S}+} + i_{\mathsf{S}-}) + V_{\mathsf{dm}}(i_{\mathsf{S}+} - i_{\mathsf{S}-}) = -i_{\mathsf{out}} \cdot e_{\mathsf{out}} - P_{\mathsf{diss}} \\
\overset{i_{\mathsf{out}} \neq 0}{\iff}\ & V_{\mathsf{cm}} + V_{\mathsf{dm}} \left(\frac{i_{\mathsf{S}+} - i_{\mathsf{S}-}}{i_{\mathsf{S}+} + i_{\mathsf{S}-}} \right) = e_{\mathsf{out}} - \frac{P_{\mathsf{diss}}}{i_{\mathsf{out}}}.
\end{aligned}$$

□

B. FIXED-POINT CONVERGENCE

According to the Banach fixed-point theorem, existence and uniqueness of the solution are guaranteed if the fixed point (55) is contracting, i.e. there exists a Lipschitz constant $\alpha \in [0, 1)$ such that

$$\left\| \phi(\mathbf{x}_1) - \phi(\mathbf{x}_0) \right\| \leq \alpha \|\mathbf{x}_1 - \mathbf{x}_0\| . \tag{59}$$

A sufficient (but conservative) condition is given by

$$\alpha = 1.162\, G\omega_d < 1. \tag{60}$$

Proof. Using (54), then the derivative of the discrete gradient (50), (bounded by $G/2$), and using the matrix norm of $\mathbf{F}_d\mathbf{C}$, one gets

$$\begin{aligned}
\left\| \phi(\mathbf{x}_1) - \phi(\mathbf{x}_0) \right\|_2 &= \left\| \mathbf{F}_d \left(\overline{\nabla} N(\mathbf{C}\mathbf{x}_0, \mathbf{C}\mathbf{x}_1) - \nabla N(\mathbf{C}\mathbf{x}_0) \right) \right\|_2 \\
&\leq \left\| \mathbf{F}_d \frac{\partial \overline{\nabla} N}{\partial v_1} \mathbf{C} \right\|_2 \|\mathbf{x}_1 - \mathbf{x}_0\|_2 \\
&\leq \|\mathbf{F}_d\mathbf{C}\|_2 \sup_{v_1} \left| \frac{\partial \overline{\nabla} N}{\partial v_1}(v_0, v_1) \right| \|\mathbf{x}_1 - \mathbf{x}_0\|_2 \\
&\leq \frac{2\omega_d \sqrt{\omega_d^2 + 8\omega_d + 20}}{\left|\omega_d^2 + 2(3-G)\omega_d + 4\right|} \frac{G}{2} \|\mathbf{x}_1 - \mathbf{x}_0\|_2 \\
&\leq 1.162\, G\omega_d \|\mathbf{x}_1 - \mathbf{x}_0\|_2
\end{aligned}$$

where the bound 1.162 is obtained numerically by majorizing over $G \in [0, 3]$ and $\omega_d \geq 0$. □